Soil Dynamics and Earthquake Engineering 129 (2020) 105969

Contents lists available at ScienceDirect

Soil Dynamics and Earthquake Engineering

journal homepage: http://www.elsevier.com/locate/soildyn

Responses of reinforced soil retaining walls subjected to horizontal and vertical seismic loadings

Cheng Fan [a], Huabei Liu [a,*], Jianzhou Cao [a], Hoe I. Ling [b]

[a] School of Civil Engineering and Mechanics, Huazhong University of Science and Technology, Wuhan, Hubei 430074, China
[b] Department of Civil Engineering and Engineering Mechanics, Columbia University, New York, NY 10027, USA

ARTICLE INFO

Keywords:
Geosynthetics
Reinforced soil retaining wall
Vertical seismic loading
Arias intensity
Seismic responses

ABSTRACT

Vertical ground acceleration is a component in an earthquake loading, and in some cases, the vertical to horizontal acceleration ratio (V/H ratio) may be very large. However, the influences of the vertical seismic loading on the responses of reinforced soil retaining walls are still not clear. In this study, a Finite Element procedure was further validated by a large-scale shaking table test subjected to both horizontal and vertical seismic loadings. It was then employed to investigate the seismic responses of two models considering a large range of earthquake loading scenarios. The results showed that the vertical ground acceleration might alter the shear wave propagation in the reinforced soil, but the Arias intensity at the top of the reinforced soil correlated well with the maximum reinforcement load. The vertical seismic loading mostly increased the reinforcement load, but reduced the residual facing displacement. The reduction of lateral facing displacement may have come from the increase of the confining pressure and the change in the far-field lateral displacement due to the vertical seismic loading. Some limitations of the present study are also discussed.

1. Introduction

A large number of geosynthetic-reinforced soil (GRS) retaining walls have been constructed in recent years [1]. The excellent seismic performances in strong earthquakes around the world have demonstrated their suitability for critical infrastructure applications in earthquake active areas [2–13]. In some of these earthquakes, especially the Northridge Earthquake and Chi-Chi Earthquake, there was a significant vertical component in the strong ground motion. However, although the static behavior of GRS retaining walls have been investigated extensively [14–28], which has helped to considerably improve the engineering practice, relatively limited studies can be found that target the dynamic behavior. Among the previous studies, reduced-scale, large--scale or centrifuge model tests on GRS structures provided the first-hand understanding on the seismic or dynamic behavior [29–37], while calibrated numerical analyses could result in in-depth knowledge of the dynamic mechanisms [38–55]. Limit equilibrium approaches have also been proposed to analyze the seismic stability of reinforced soil structures [56–60]. From these studies, it have been found that GRS retaining walls generally demonstrated good performance under strong earthquake loading, but proper seismic design is still necessary.

Most design practices at present treat the seismic loading as certain inertia forces, while some design guidelines take into account the influence of wall height [61,62]. However, some studies showed that the frequency characteristics of the input ground motion and the fundamental frequency of the GRS structure are important variables that may determine the seismic responses [43,50–53,63–65]. The frequency characteristics couple with the natural resonant frequency of the GRS structure, and the structure may behave very much differently with the same input of horizontal peak acceleration. Liu et al. [53] further found that the Arias intensity of the input ground motion is another critical parameter that determined the seismic behavior, and considering both the frequency characteristics and Arias intensity of the input motion yielded the best correlation with the seismic responses. The use of Arias intensity to link wall displacements to earthquake intensity has been used for conventional structures [66]. Another essentially identical property to the Arias intensity, the RMS value, which has been used to equate earthquake intensity to GRS wall face displacements [29], is not discussed in this study.

The influence of vertical ground motion is a subject that deserves much attention, particularly for a GRS structure located close to an active fault [67]. Through limit equilibrium analyses, Ling and Leshchinsky [56] showed that upward and downward vertical accelerations

* Corresponding author.
E-mail addresses: fancl130@163.com (C. Fan), hbliu@hust.edu.cn (H. Liu), a5580399@qq.com (J. Cao), hil9@columbia.edu (H.I. Ling).

https://doi.org/10.1016/j.soildyn.2019.105969
Received 3 January 2019; Received in revised form 2 May 2019; Accepted 11 November 2019
Available online 17 November 2019

Nomenclature

I_a	Arias intensity
T_d	Duration of the horizontal earthquake motion
$a(t)$	Time history of the horizontal acceleration
g	Gravity constant
T_{max}	Maximum reinforcement load
δ_{max}	Maximum lateral facing displacement
p'	Effective mean stress of soil
q	Deviator stress
p_{atm}	Atmosphere pressure
$\mathbf{D}^e$	Elastic rigidity matrix
$\mathbf{n}_{gL/U}$	Plastic flow direction
$\mathbf{n}$	Loading direction
$H_{L/U}$	Plastic modulus in loading or unloading
φ_0	Reference friction angle of soil at p' = 100 kPa
$\Delta\varphi$	Change of friction angle with pressure
M_g	Critical state stress ratio in triaxial compression
M_f	Model parameter for loading direction vector of sand
G_{max}	Shear modulus
K_{max}	Bulk modulus
G_0	Shear modulus parameter
K_0	Bulk modulus parameter
α	Stress-dilatancy parameter
H_0	k_s, β_{10}, β_0 Generalized plasticity model parameters defining loading plastic modulus
H_{u0}	and r_u Generalized plasticity model parameters defining unloading plastic modulus
r_d	Generalized plasticity model parameter controlling cyclic hardening of soil
r	Generalized plasticity model parameter controlling the influence of stress history
ξ	Accumulative plastic shear strain

imposed different requirements on the reinforcements: upward acceleration would increase reinforcement loads, while downward acceleration required larger reinforcement length for stability. Similar findings were also reported by Ling and Leshchinsky [68], Nimbalkar et al. [57], Choudhury et al. [58], Shekarian et al. [69], Basha and Babu [70], and Vahedifard et al. [71] using different limit-equilibrium approaches. Some of these analyses also found that keeping the same vertical to horizontal (V/H) ratio of the seismic coefficients, the influence of the vertical seismic coefficient was only significant when the horizontal one was adequately large [56,71]. However, some studies pointed out that using only a vertical seismic coefficient might not be adequate, as the phase difference between the horizontal and vertical motions affected the seismic responses considerably [72,73].

While many simplistic analyses on the influences of vertical seismic motions can be found in the literature, large-scale experimental investigations or reliable numerical simulations are quite limited [74]. Ling et al. [30] carried out a series of large-scale shaking table tests to investigate the seismic responses of GRS retaining walls. Vertical ground motion was considered in one of the tests. Using actual records of horizontal and vertical ground motions from the 1995 Kobe earthquake, it was found that the vertical ground motion did not affect the facing displacement considerably, but it resulted in higher reinforcement loads. Ling et al. [44] and Lee et al. [75] later simulated the shaking table tests using Finite Element method. It should be noted that the model walls in the shaking table tests were only 2.8 m high, and had a limited length beyond the reinforced soil zone [65]. Therefore the influence of the wall flexibility, which may couple with the vertical ground motion, cannot be clearly identified. Flexibility of the facing is not considered in closed-form static working stress methods with the exception of the Simplified Stiffness Method and its antecedents [76,77].

In this study, the Finite Element procedure in Liu et al. [47] was further validated against the large-scale shaking test with vertical excitation in Ling et al. [30]. Dynamic Finite Element analyses were then carried out on two model walls, the heights of which were 6 m and 9 m, respectively. The model walls were subjected to both horizontal and vertical seismic loadings. Altogether 23 sets of strong ground motion records from the 1999 Chi-Chi Earthquake and the 1979 Imperial Valley Earthquake were employed as the seismic excitations. The dynamic responses were compared to the ones with horizontal seismic loadings only, which were reported in Liu et al. [53].

2. Finite element procedure and its validation

The dynamic Finite Element procedure was updated from the version in Ling et al. [41,42]. In this procedure, the nonlinear dynamic Finite Element code Swandyne-II was used [43,78,79]. The backfill soil was assumed to be cohesionless and modeled by a generalized plasticity model [80], a brief introduction of which is given in the Appendix. The reinforcement-soil interfaces were modeled by thin-layer elements, the constitutive responses of which were also captured by the generalized plasticity model but with reduced shear strength and stiffness [47]. The geosynthetic reinforcements were modeled by three-node bar elements and assumed to be linear elastic. Previous experimental studies have shown that geosynthetic reinforcements are rate-sensitive and exhibit hysteretic stress-strain behavior under cyclic loading [81]. However, dynamic Finite Element analyses showed that the hysteretic behavior did not considerably affect the seismic response [79], and a secant value could properly capture the effect of reinforcement stiffness [76,77]. Concrete modular block facing was assumed in the numerical models. The concrete blocks were assumed to be linear elastic with $E = 2.0 \times 10^6$ kPa and $\nu = 0.2$, the same as those in Ling et al. [44]. The blocks were 20 cm high and 30 cm deep and their unit weight is assumed to be 18 kN/m^3 since the hollow portion of the blocks was filled with gravel and compacted. The interfaces between the blocks, those between the soil and the blocks and those between geogrids and the blocks were modeled by thin-layer elements that follow the Mohr-Coulomb failure criterion [82]. The soil–block interfaces ($\delta = 27°$), block–block interfaces ($\delta = 35°$) and block–geogrid interfaces ($\delta = 35°$) were modeled in the same way as those in Ling et al. [44], the frictional angles of which were determined from direct shear tests [83]. The numerical analysis is completed in two steps: the static responses are firstly obtained by construction simulation [41,79], followed by a dynamic analysis to capture the seismic behavior. Construction simulation was carried out by continuously activating the block, soil, reinforcement, and interface elements layer by layer, while the compaction effect was not simulated. Neglecting the compaction effect in the dynamic analyses has led to smaller facing displacement in the first shaking, which will be discussed in the subsequent paragraph. The acceleration time-history of the ground motion is input at the base of the model. Time-domain dynamic analysis is carried out using the generalized Newmark method, and a viscous damping of 5% is considered in the dynamic analysis. Further details can be found in Ling et al. [41,42] and Liu et al. [47].

Wall 3 in Ling et al. [30] was employed to further validate the Finite Element procedure for the dynamic analysis considering vertical seismic excitation. Fig. 1 shows the Finite Element mesh. The model parameters of the backfill soils are presented in Table 1, which were calibrated from cyclic triaxial compression tests on Tokachi sand (D_r = 55%) as reported in Liu et al. [47], The 0.2 m thick foundation used the same soil but at a relative density of 90%. In the shaking table test, the top reinforcement layer was one type of PVA geogrid, which was different from

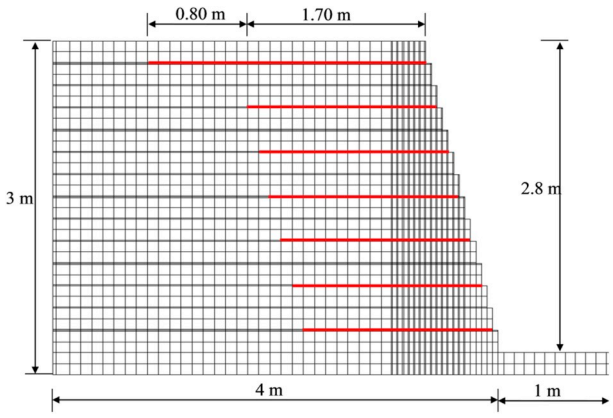

Fig. 1. Finite Element mesh for the test wall.

the other layers. The reinforcement stiffness of the top layer was 500 kN/m, while that of the other layers were 400 kN/m. These values were interpreted from the tensile test results reported in Ling et al. [44], which represented the secant stiffness at a strain of 2%. The model wall was subjected to two consecutive shakings, and the actual input accelerations in the shaking table test were used. In the second shaking, the peak horizontal acceleration was 0.83 g, while the peak vertical acceleration was 0.38 g. The input accelerations in the first shaking were approximately half of those in the second one. According to Ling [84], the fundamental frequency of a 3-m wall was about 7.25 Hz. The predominant frequency of the North–South (NS) and Up-Down (UD) components of the Kobe earthquake records were 0.98 Hz and 1.08 Hz, respectively, which were far away from the fundamental frequency of the structure. The details of the input motions can be found in Ling et al. [33,40].

Fig. 2 shows the comparisons between the results from the test and the Finite Element method (FEM). It can be seen that the Finite Element procedure satisfactorily reproduced the overall responses of the GRS retaining wall in the shaking table test. The facing displacement after the first shaking was very small in the test, which might be due to the compaction effect in the backfill soil [85] but was not captured by the model parameters since they were calibrated from triaxial tests. In addition, the Finite Element procedure could not reproduce the large connection loads in two reinforcement layers, as shown in Fig. 2c. According to Ling et al. [30], relative settlement between the backfill soil and blocks due to backfill compression led to geogrid overhanging at the connection, and void spaces were observed beneath the geogrid at the back of facing [86]. Overhanging of some reinforcement layers at connection might have resulted in the large connection load, but such behavior cannot be captured by a Finite Element procedure that is based on continuum mechanics. The connection loads were also underestimated in the Finite Element analyses by Ling et al. [44] and Lee et al. [75].

It should be pointed out that in the Finite Element simulation, the shear keys of the blocks were not directly modeled, which could result in larger facing displacements and reinforcement loads to some extent.

3. Finite Element models

The seismic responses of two model GRS retaining walls were investigated. The heights were 6 m and 9 m, respectively. In order to minimize influence of the side boundaries, the backfill soil extended 55 m beyond the back of the reinforced soil. Finite Element meshes of the model walls were the same as those in Liu et al. [53]. The foundation soil is assumed to be underlain by stiff rock, hence the Finite Element model is fixed at the base, and roller boundaries are used on the sides. Vertical modular block facings were assumed, the unit weight of which was 24 kN/m^3. Dense Toyoura sand was used as the backfill soil, and the parameters are shown in Table 1 [53]. The stiff geogrid reinforcements were assumed to be elastic with a stiffness of 1300 kN/m, which were placed between facing blocks to provide the connection strength. The reinforcement spacing was 60 cm for the 6 m wall, and 40 cm for the 9 m wall. The reinforcement length was 70% of the wall height beyond the back of facing.

The interfaces between backfill soil and geogrid reinforcements were simulated by the thin-layer elements together with the same generalized plasticity model for sand. The shear modulus, bulk modulus, plastic modulus, peak stress ratio, and critical-state stress ratio were all assumed to be 2/3 of the adjacent backfill soil, while the other parameters were assumed to be the same.

After obtaining the static response through construction simulation [79], the model walls were subjected to the base excitations. Altogether 23 strong ground motions were employed in the analyses, which were taken from the records of the 1999 Chi-Chi Earthquake or those of the 1979 Imperial Valley Earthquake. All the input horizontal motions were scaled to have a peak acceleration of 0.4 g, and the corresponding vertical motions were scaled proportionally according to the actual V/H ratio.

Table 2 shows the characteristics of the input motions. Here "C" represents the Chi-Chi Earthquake, and "I" represents the Imperial Valley Earthquake. The number is the station number used in the PEER Ground Motion Database. The Arias intensity I_a is defined as:

$$I_a = \frac{\pi}{2g}\int_0^{T_d} a(t)^2 dt \tag{1}$$

Here T_d is the duration of the horizontal earthquake motion, $a(t)$ is the time history of the horizontal acceleration, and g is the gravitational constant. It should be noted that only fourteen (14) analyses were carried out on the high wall. The predominant period is around 0.22–0.25s for the 6 m wall and around 0.35–0.4s for the 9 m wall. Since the 14 input motions selected for the high wall covered a wide range of predominant frequency and Arias intensity, the results obtained are believed to be representative for the structure.

The other parameters of the Finite Element models can be found in Liu et al. [53].

4. Results

The maximum horizontal accelerations at the top of the reinforced soil zone are summarized in Table 3. It can be seen that although the peak values of the input horizontal accelerations were the same, the acceleration amplifications in the reinforced soil zone were very different. In particular, the response of the model wall subjected to the excitation of C1491 was much larger than those of the others.

As shown in Fig. 3, typical results of lateral facing displacements are selected to demonstrate their characteristics. It can be seen that when the seismic responses were small, the maximum facing displacement was found around the mid height of the wall, as it was mainly the displacement under static loading. However, the lateral facing

Table 1
Model parameters for the backfill soil and the soil-geogrid interface.

	φ_0[°]	$\Delta\varphi$[°]	M_g	M_f	$G_0[p_{atm}]$	$K_0[p_{atm}]$	k_s	β_{10}	β_0	α	$H_0[p_{atm}]$	$H_{u0}[p_{atm}]$	r	r_u	r_d
Backfill soil	43.7	4.9	1.25	0.688	861	886	0.015	1.1	15	0.5	5000	4000	3	1	3000
Soil-geogrid interface	32.5	3.3	0.83	0.459	1513	1513	0.015	1.1	15	0.5	3333	2667	3	1	3000

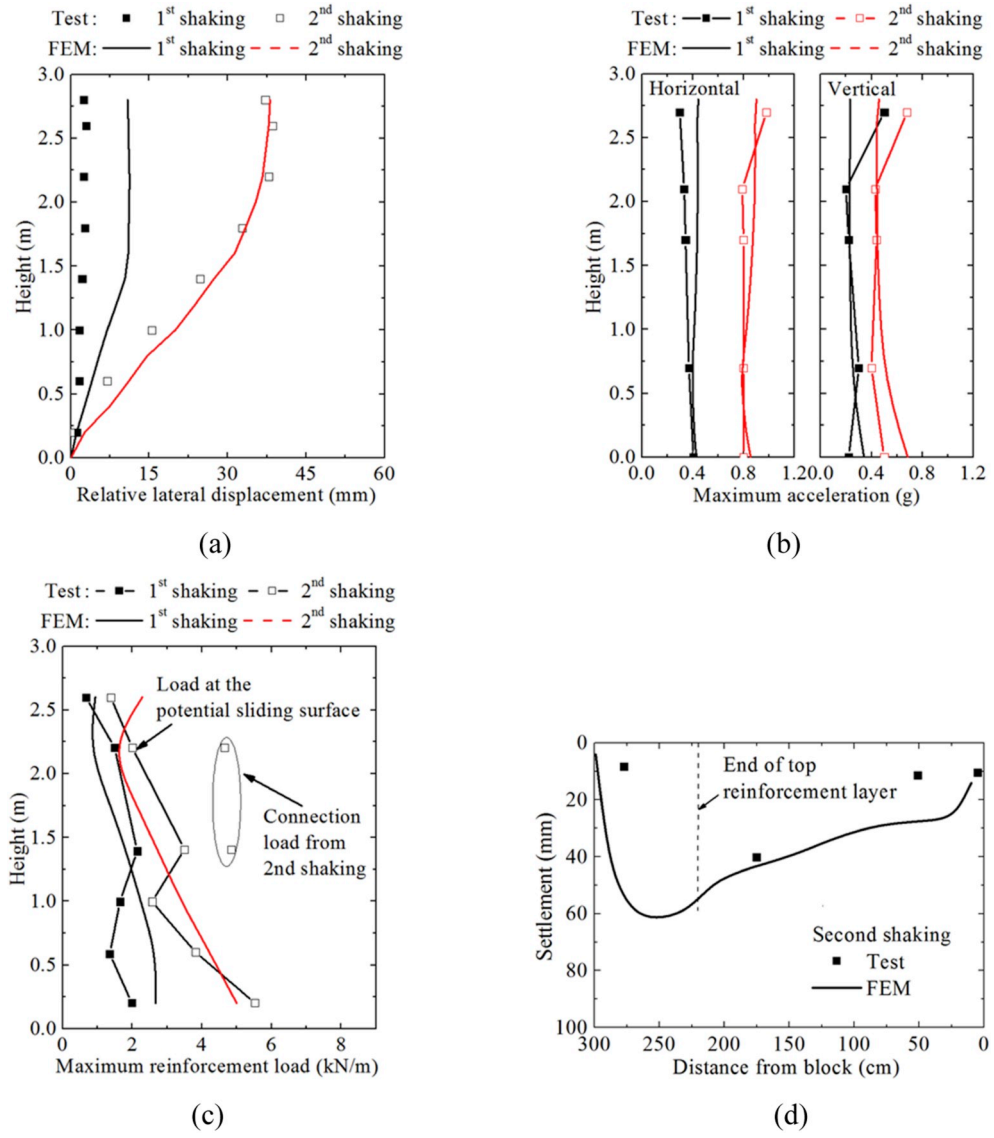

Fig. 2. Comparisons between test and Finite Element Method (FEM) results: (a) Lateral facing displacement; (b) Acceleration amplification; (c) Maximum reinforcement load; (d) Backfill surface settlement.

Table 2
Characteristics of the input motions.

Input motion	C1182	C1193	C1244	C1402	C1476	C1477	C1480	C1481	C1482	C1483	C1487
Predominant period/s	0.45	0.4	0.15	0.2	0.45	0.65	0.3	0.75	0.55	0.4	0.95
Arias intensity (m/s)	1.846	3.671	3.203	1.158	3.689	5.080	6.256	3.952	3.880	3.947	2.579
Vertical acceleration (g)	0.240	0.204	0.195	0.114	0.161	0.232	0.182	0.185	0.252	0.199	0.357

Input motion	C1489	C1491	C1492	I159	I161	I170	I171	I173	I179	I180	I184	I185
Predominant period/s	0.2	0.3	1.1	0.55	0.25	0.5	0.65	0.5	0.2	0.35	0.15	0.35
Arias intensity (m/s)	2.758	7.622	3.575	1.762	1.842	2.666	1.370	3.091	0.917	1.217	2.234	2.108
Vertical acceleration (g)	0.261	0.280	0.220	0.658	0.375	0.462	0.314	0.254	0.241	0.449	0.873	0.398

displacement close to the top of the wall became the largest when the seismic responses were much larger, similar to the findings in the large-scale shaking table tests by Ling et al. [30]. As discussed in Liu et al. [53], the lateral facing displacement included the contribution from the far field displacement of the retained soil. In some cases, the residual far-field displacement was actually in the opposite direction, and overall the lateral facing displacement was not large.

The typical results of the maximum reinforcement load distributions are presented in Fig. 4. The distributions of the reinforcement loads were similar to the ones under vertical loading only [53], although the magnitudes were different.

Fig. 5 shows the relationships between the maximum reinforcement load and the horizontal Arias intensity at the top of the reinforced soil zone. For comparison purposes, the responses under horizontal loading only reported in Liu et al. [53] are also shown in these figures. It can be seen that for both of the model walls, the correlations between the maximum reinforcement load and the horizontal Arias intensity are very good, further confirming the finding in Liu et al. [53]. It should be noted

Table 3
Maximum horizontal accelerations at the top of the reinforced soil zone.

Input motion	C1182	C1193	C1244	C1402	C1476	C1477	C1480	C1481	C1482	C1483	C1487	C1489
Height (m)	6	6	6	6	6	6	6	6	6	6	6	6
Maximum horizontal accelerations (g)	0.527	0.774	0.629	0.774	0.804	0.588	0.685	0.620	0.525	0.591	0.623	0.789
Input motion	C1491	C1492	I159	I161	I170	I171	I173	I179	I180	I184	I185	–
Height (m)	6	6	9	9	9	9	9	9	9	9	9	–
Maximum horizontal accelerations (g)	1.051	0.527	0.536	0.718	0.785	0.677	0.701	0.558	0.769	0.753	0.839	–

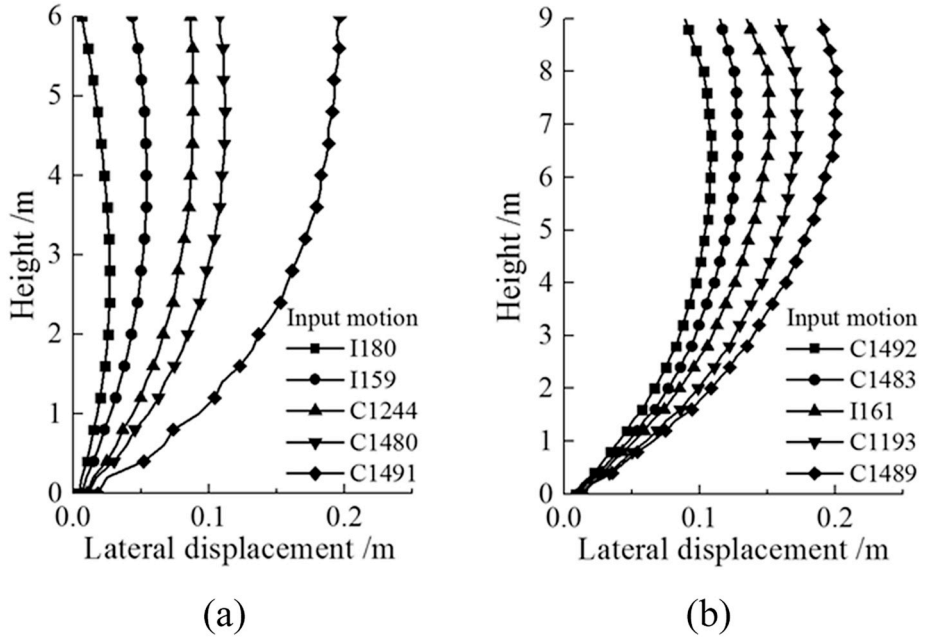

Fig. 3. Typical residual lateral facing displacements: (a) 6 m wall; (b) 9 m wall.

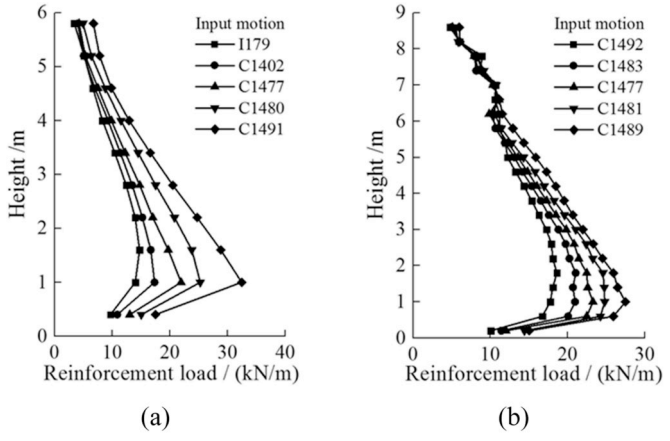

Fig. 4. Typical maximum reinforcement load distributions: (a) 6 m wall; (b) 9 m wall.

that the retaining wall is assumed to be underlain by stiff rock, and the correlations could be different if the retaining wall is on a soil site.

The influences of the vertical excitations are discussed by making use of the results in this study and those in Liu et al. [53], as shown in Fig. 6 and Fig. 7. It can be seen from Fig. 6 that the vertical excitations in this study mostly increased the horizontal seismic accelerations at the top of the reinforced soil zones, indicating that the characteristics of shear wave propagations in the walls were modified by the vertical excitations. The larger horizontal seismic accelerations led to larger maximum reinforcement loads, as shown in Fig. 7a. However the maximum lateral facing displacements with vertical excitations were mostly smaller, while the settlements at the reinforced soil surface were slightly larger, as shown in Fig. 7b and c, respectively.

5. Discussions

The results in this study further show that in order to accurately capture the response of a reinforced soil retaining wall subjected to earthquake loading, it is necessary to take into account the vibration property of the earth structure, the frequency characteristics of the input motion, and the duration of the input motion, in addition to the peak ground acceleration. The acceleration intensity response, represented by the Arias intensity, at the top of the reinforced soil, very well captures the seismic loading characteristics on the reinforced soil retaining wall. Vertical seismic excitation could alter the confining pressure on the backfill soil, influence the soil stiffness, and modify the shear wave propagation in the reinforced soil. Its effect on the reinforcement load can be mostly captured by the change in the Arias intensity due to the change in the shear wave propagation.

As previously pointed out, vertical ground acceleration generally increased the confining pressure and the soil stiffness, which partly led to the smaller lateral facing displacements, as shown in Fig. 7b, but the reinforced soil compression was slightly higher. This finding is consistent with the test result in Ling et al. [30]. The change in the soil stiffness also modified the vibration of the free field, and the far-field displacements might be different with two types of earthquake excitations. Fig. 8 shows the comparisons of the far-field displacements of two earthquake scenarios. It can be seen that for these scenarios, the far-field

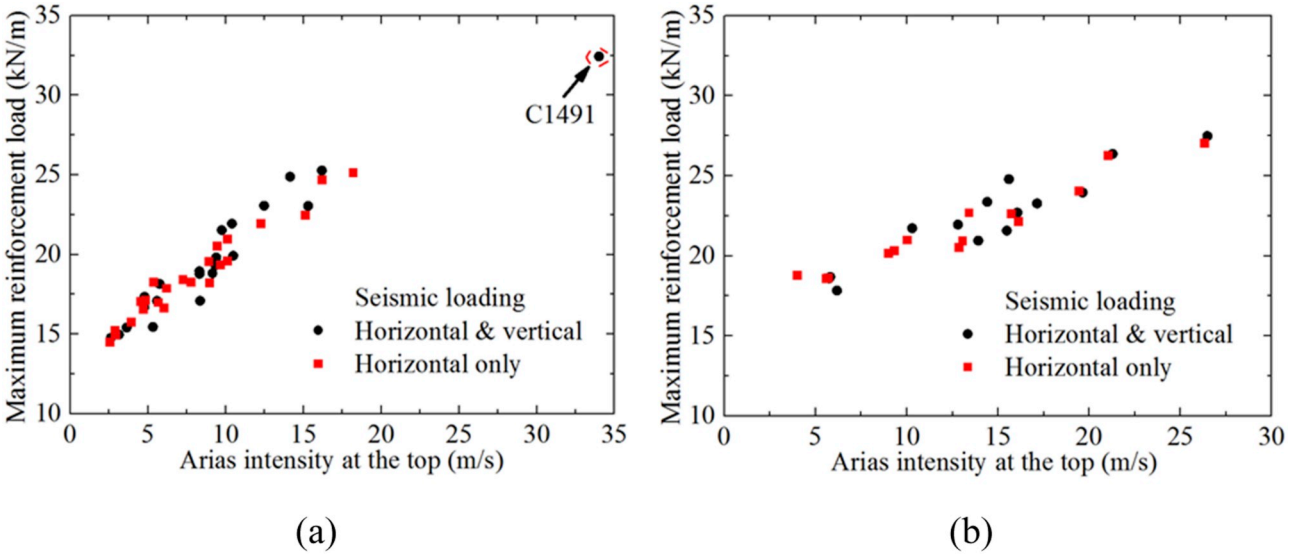

Fig. 5. Relationship between maximum reinforcement load and Arias intensity at the top of reinforced soil: (a) 6 m wall; (b) 9 m wall.

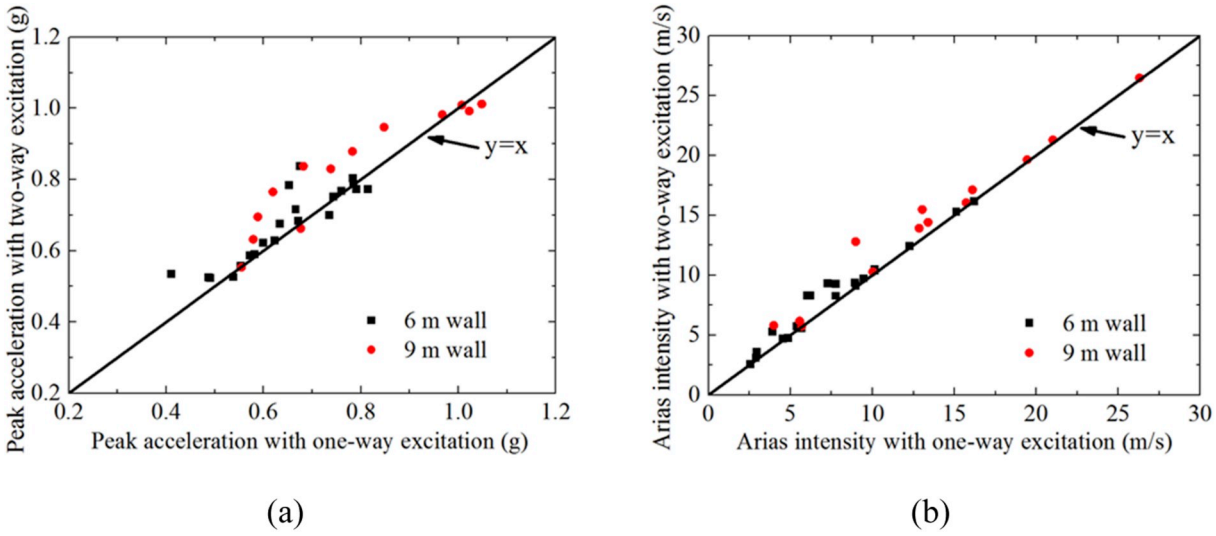

Fig. 6. Influence of vertical acceleration on the horizontal acceleration at the top: (a) peak acceleration; (b) Arias intensity.

displacements with the vertical excitation actually reduced the lateral facing displacements considerably.

The study also highlighted the importance of boundary condition in the seismic analysis and design of reinforced soil structures. In this study, the retained soil was assumed to be adequately deep so that the free field response can be assumed at the side boundary. Clearly the seismic displacements of the retained soil and the back boundary influenced the residual displacement of the earth retaining structures. The residual facing displacements might be different with different back boundaries, which was also reported in Bathurst and Hatami [65]. A reasonable approach to take into account the side boundary is called for in the residual displacement analysis of reinforced soil retaining structures subjected to seismic loading.

The Finite Element procedure of this study could not capture the possible large connection load due to vertical ground excitation. In this study, the soil-block interfaces were simulated by thin-layer elements, and the continuum characteristics of the Finite Element models make it difficult to reproduce the possible large relative movement between the backfill soil and the facing blocks under large vertical excitation. More advanced numerical approach, which may capture the large relative movements among backfill soil, facing blocks, and reinforcement layers, is necessary to fully understand the increase of reinforcement load as well as its mechanism. The foundation soil was assumed to be thin in this study, and under similar earthquake loading the overall wall deformations may increase to some extent with an increase in the depth of the foundation soil. The depth of foundation soil also affects the wave propagation into the retaining wall. However, this study is focused on the dynamic responses in the wall body, and the predominant frequency of the seismic loading considered had a large range. Therefore, it is believed that the correlation obtained would apply to more general ground conditions.

6. Conclusions

In this study, a Finite Element procedure for the seismic behavior of reinforced soil retaining walls was further validated against a large-scale shaking table test. It was demonstrated that the procedure were able to capture the dynamic responses of GRS retaining walls subjected to both horizontal and vertical earthquake shakings with an acceptable accuracy. The responses of two reinforced soil model walls were then

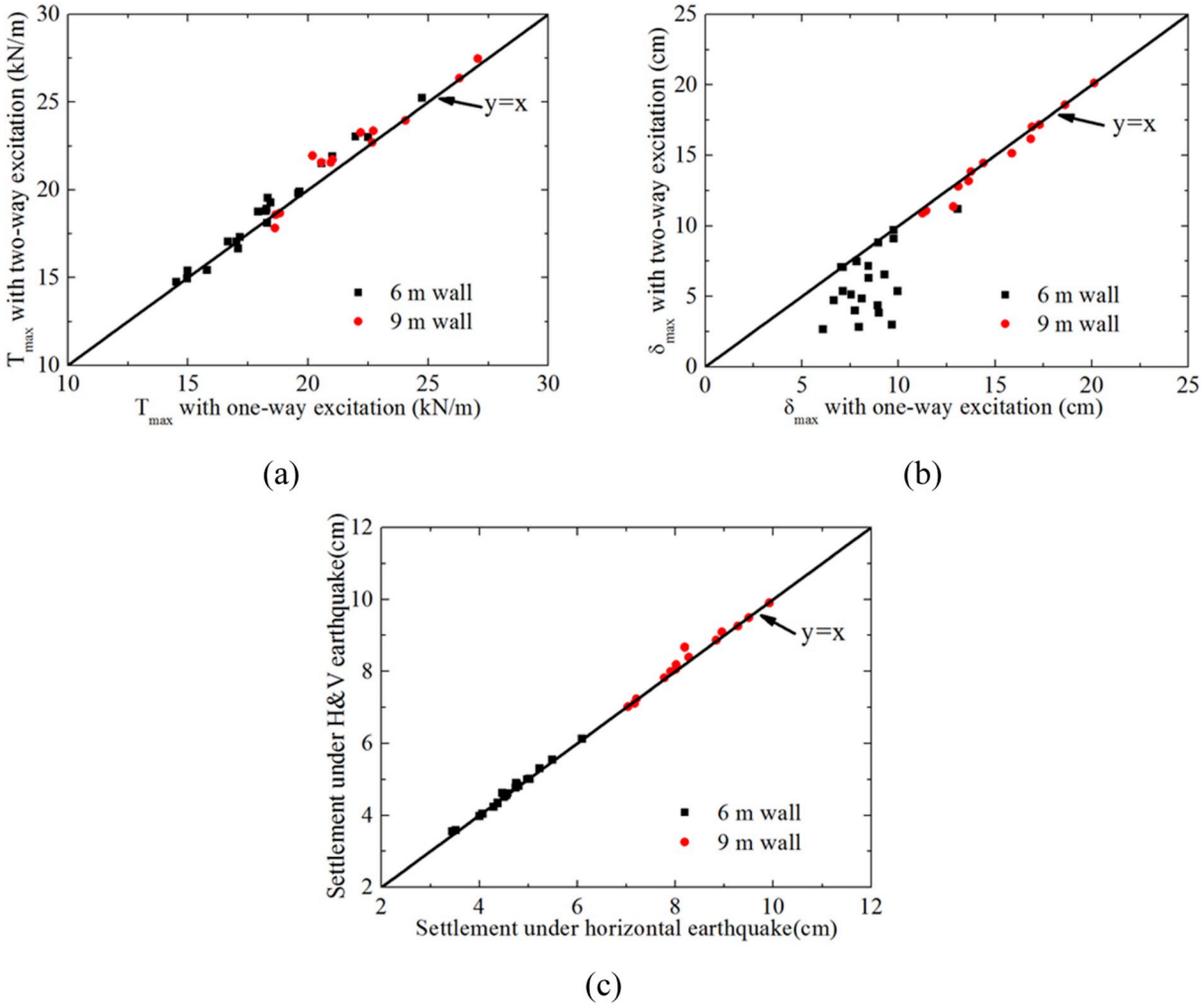

Fig. 7. Influence of vertical acceleration on the wall responses: (a) maximum reinforcement load; (b) residual lateral facing displacement; (c) settlement at the top of reinforced soil.

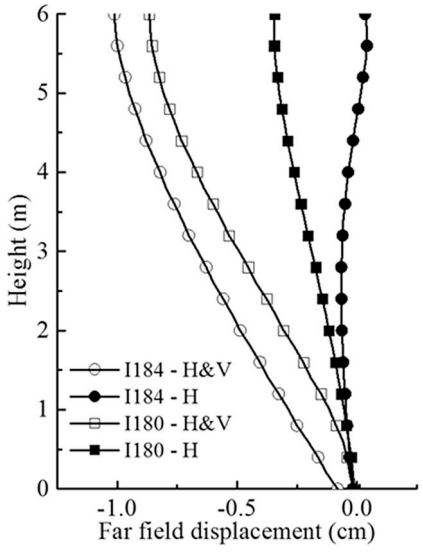

Fig. 8. Comparisons of the far-field displacements with or without vertical excitations.

analyzed considering a wide range of earthquake loadings. The results showed that vertical earthquake loading could increase the reinforcement load, but the lateral facing displacement might be larger if the structure was subjected to horizontal earthquake loading only. The vertical excitation altered the shear wave propagation in the reinforced soil wall, and changed the amplification of the seismic acceleration, which might result in higher acceleration intensity in the earth structure. The correlation between the maximum reinforcement load and the Arias intensity at the top of the reinforced soil was very good for the cases of one-way or two-way earthquake loading.

The study shows that using a peak acceleration to analyze the maximum reinforcement load without considering the excitation intensity and frequency content may not be adequate in the design of GRS retaining walls. The records from recent strong earthquakes have shown that the duration, intensity and frequency content may vary significantly in the ground motions, even if the peak accelerations are similar. The intensity and frequency content are also considerably affected by the ground condition and the associated wave propagation.

Acknowledgements

The study was supported by the National Natural Science Foundation of China (Grant No. 51778259), which is gratefully acknowledged.

Appendix B. Supplementary data

Supplementary data to this article can be found online at https://doi.org/10.1016/j.soildyn.2019.105969.

Appendix A

In this constitutive model for sand, the elasto-plastic rigidity matrix is written as:

$$\mathbf{D}^{ep} = \mathbf{D}^{e} - \frac{\mathbf{D}^{e} : \mathbf{n}_{gL/U} : \mathbf{n}^{T} : \mathbf{D}^{e}}{H_{L/U} + \mathbf{n}^{T} : \mathbf{D}^{e} : \mathbf{n}_{gL/U}} \tag{A-1}$$

in which $\mathbf{D}^{e}$ is the elastic rigidity matrix, $\mathbf{n}_{gL/U}$ is the plastic flow direction, $\mathbf{n}$ is the loading direction, and $H_{L/U}$ is the plastic modulus in loading or unloading. The shear and bulk elastic moduli are given as:

$$G_{\max} = G_0(p'/p_{atm})^{0.5}, \quad K_{\max} = K_0(p'/p_{atm})^{0.5} \tag{A-2}$$

in which p' is the mean effective stress, p_{atm} is the atmosphere pressure, and G_0 and K_0 are model parameters. The plastic-flow direction vectors are defined in triaxial space as:

$$\mathbf{n}_{gL} = \left(\frac{d_g}{\sqrt{1+d_g^2}}, \frac{1}{\sqrt{1+d_g^2}} \right)^{T} \tag{A-3a}$$

$$\mathbf{n}_{gU} = \left[-abs\left(\frac{d_g}{\sqrt{1+d_g^2}} \right), \frac{1}{\sqrt{1+d_g^2}} \right]^{T} \tag{A-3b}$$

where:

$$d_g = (1+a)\left(M'_g - \frac{q}{p'} \right) \tag{A-4}$$

Here q is the deviatoric stress, M'_g is the critical state shear stress ratio and function of the residual angle of internal friction φ_{cv}, and α is a model parameter. The plastic flow of granular soil is assumed to be non-associative and the loading-direction vector is expressed in the triaxial space as:

$$\mathbf{n} = \left(\frac{d_f}{\sqrt{1+d_f^2}}, \frac{1}{\sqrt{1+d_f^2}} \right)^{T} \tag{A-5}$$

with

$$d_f = (1+\alpha)\left(M_f - \eta \right) \tag{A-6}$$

The plastic moduli under loading and unloading are respectively defined as:

$$H_L = H_0(p'/p_{atm})^{0.5}\left(1 - \frac{\eta}{\eta_f} \right)^{4} \left\{ 1 - \frac{\eta}{M_g} + H_s \right\} \exp(-r_d \varepsilon_{v0}^{p}) H_{DM} \tag{A-7a}$$

$$H_U = H_{u0}(p'/p_{atm})^{0.5}\left(\frac{M_g}{\eta} \right)^{r_u} \exp(-r_d \varepsilon_{v0}^{p}) \tag{A-7b}$$

in which

$$H_s = \beta_1(p', \eta)\exp(-\beta_0 \xi)\exp\{k_s(p'/p_{atm} - 1)\} \tag{A-8}$$

Here ξ is the accumulative plastic shear strain. The detailed calibration procedure can be found in Ling and Liu [64].

References

[1] Kongkitkul W, Tatsuoka F, Hirakawa D, Sugimoto T, Kawahata S, Ito M. Time histories of tensile force in geogrid arranged in two full-scale high walls. Geosynth Int 2010;17(1):12–33.

[2] Koseki J. Use of geosynthetics to improve seismic performance of earth structures. Geotext Geomembranes 2012;34:51–68.

[3] Seed RB. Preliminary report on the principal geotechnical aspects of the October 17, 1989, Loma Prieta earthquake. Report No. UCB/EERC-90/05. 1990.

[4] Eliahu U, Watt S. Geogrid-reinforced wall withstands earthquake. IFAI (2) Geotech Fabr Rep 1991;9:8–13.

[5] Stewart JP, Bray JD, Seed RB, Sitar N. Preliminary report on the principal geotechnical aspects of the January 17, 1994 Northridge earthquake. University of California, Berkeley, earthquake engineering research center. Report UCB/EERC-94/08. 1994.

[6] Sandri D. A summary of reinforced soil structure performance in the greater Los Angeles area after the Northridge earthquake. In: Wu J, editor. Mechanically stabilized backfill. Rotterdam, The Netherlands: Balkema; 1997. p. 433–42.

[7] Akai K, Bray JD, Christian JT, Boulanger RW. Geotechnical reconnaissance of the effects of the January 17, 1995, Hyogoken-Nanbu earthquake. Japan: DIANE Publishing; 1997.
[8] Ling HI, Leshchinsky D, Chou NNS. Post-earthquake investigation on several geosynthetic-reinforced soil retaining walls and slopes during 1999 Ji-Ji Earthquake of Taiwan. Soil Dyn Earthq Eng 2001;21(4):297–313.
[9] Abrahamson JP, Bardet R, Boulanger J, Bray YW, Chan CY, Chang CH. Preliminary geotechnical earthquake engineering observations of the September 21, 1999, Chichi, Taiwan earthquake. 2003.
[10] Huang CC, Chou LH, Tatsuoka F. Seismic displacements of geosynthetic-reinforced soil modular block walls. Geosynth Int 2003;10(1):2–23.
[11] Ansal A, Bardet JP, Bray J, Cetin O, Durgunoglu T, Erdik M, et al. Initial geotechnical observations of the August 17, 1999, izmit earthquake. A report of the Turkey–US reconnaissance team. 1999.
[12] Bray JD, Sancio R, Kammerer AM, Merry S, Rodriguez-Marek A, Khazai B, et al. Some observations of the geotechnical aspects of the February 28, 2001, nisqually earthquake in olympia, South Seattle, and Tacoma, Washington. University of Arizona, Washington State University, Shannon and Wilson Inc., and Leighton and Associates; 2001. Report sponsored by NSF, PEER Center, UCB.
[13] Bray JD, Frost D. Geo-engineering reconnaissance of the February 27, 2010 Maule, Chile earthquake. Geoengineering extreme events reconnaissance (GEER). 2010.
[14] Rowe RK, Ho SK. Continuous panel reinforced soil walls on rigid foundations. J Geotech Geoenviron Eng ASCE 1997;123(10):912–20.
[15] Rowe RK, Ho SK. Horizontal deformation in reinforced soil walls. Can Geotech J 1998;35(2):312–27.
[16] Rowe RK, Skinner GD. Numerical analysis of geosynthetic reinforced retaining wall constructed on a layered soil foundation. Geotext Geomembranes 2001;19(7):387–412.
[17] Skinner GD, Rowe RK. Design and behaviour of geosynthetic reinforced soil walls constructed on yielding foundations. Geosynth Int 2003;10(6):200–14.
[18] Skinner GD, Rowe RK. Design and behaviour of a geosynthetic reinforced retaining wall and bridge abutment on a yielding foundation. Geotext Geomembranes 2005;23(3):234–60.
[19] Skinner GD, Rowe RK. A novel approach to estimating the bearing capacity stability of geosynthetic reinforced retaining walls constructed on yielding foundations. Can Geotech J 2005;42(3):763–79.
[20] Chen J, Zhang W, Xue J. Zoning of reinforcement forces in geosynthetic reinforced cohesionless soil slopes. Geosynth Int 2017;24(6):565–74.
[21] Holtz RD. 46th Terzaghi lecture: geosynthetic reinforced soil: from the experimental to the familiar. J Geotech Geoenviron Eng ASCE 2017;(9):143.03117001.
[22] Khosrojerdi M, Xiao M, Qiu T, Nicks J. Evaluation of prediction methods for lateral deformation of GRS walls and abutments. J Geotech Geoenviron Eng ASCE 2016;(2):143. 06016022.
[23] Leshchinsky D, Leshchinsky B, Leshchinsky O. Limit state design framework for geosynthetic-reinforced soil structures. Geotext Geomembranes 2017;45(6):642–52.
[24] Mirmoradi SH, Ehrlich M. Numerical simulation of compaction-induced stress for the analysis of RS walls under working conditions. Geotext Geomembranes 2018;46(3):354–65.
[25] Plácido R, Portelinha FHM, Futai MM. Field and laboratory time-dependent behaviors of geotextiles in reinforced soil walls. Geosynth Int 2018;25(2):215–29.
[26] Sadat MR, Huang J, Bin-Shafique S, Rezaeimalek S. Study of the behavior of mechanically stabilized earth (MSE) walls subjected to differential settlements. Geotext Geomembranes 2018;46(1):77–90.
[27] Saghebfar M, Abu-Farsakh M, Ardah A, Chen Q, Fernandez BA. Performance monitoring of geosynthetic reinforced soil integrated bridge system (GRS-IBS) in Louisiana. Geotext Geomembranes 2017;45(2):34–47.
[28] Wang L, Liu H, Wang C. Earth pressure coefficients for reinforcement loads of vertical geosynthetic-reinforced soil retaining walls under working stress conditions. Geotext Geomembranes 2018;46(4):486–96.
[29] El-Emam MM, Bathurst RJ. Facing contribution to seismic response of reduced-scale reinforced soil walls. Geosynth Int 2005;12(5):215–38.
[30] Ling HI, Mohri Y, Leshchinsky D, Burke C, Matsushima K, Liu H. Large-scale shaking table tests on modular-block reinforced soil retaining walls. J Geotech Geoenviron Eng ASCE 2005;131(4):465–76.
[31] Nova-Roessig L, Sitar N. Centrifuge model studies of the seismic response of reinforced soil slopes. J Geotech Geoenviron Eng ASCE 2006;132(3):388–400.
[32] Guler E, Enunlu AK. Investigation of dynamic behavior of geosynthetic reinforced soil retaining structures under earthquake loads. Bull Earthq Eng 2009;7(3):737–77.
[33] Ling HI, Leshchinsky D, Mohri Y, Wang JP. Earthquake response of reinforced segmental retaining walls backfilled with substantial percentage of fines. J Geotech Geoenviron Eng ASCE 2012;138(8):934–44.
[34] Guler E, Selek O. Reduced-scale shaking table tests on geosynthetic-reinforced soil walls with modular facing. J Geotech Geoenviron Eng ASCE 2014;(6):140.04014015.
[35] Liu H, Yang G, Wang H, Xiong B. A large-scale test of reinforced soil railway embankment with soil bag facing under dynamic loading. Geomech Eng 2017;12(4):579–93.
[36] Enomoto T, Sasaki T. Seismic behaviour of reinforced embankments in dynamic centrifuge model tests. Soils Found 2018;58(1):212–27.
[37] Yazdandoust M. Laboratory evaluation of dynamic behavior of steel-strip mechanically stabilized earth walls. Soils Found 2018;58(2):264–76.
[38] Cai Z, Bathurst RJ. Seismic response analysis of geosynthetic reinforced soil segmental retaining walls by Finite Element method. Comput Geotech 1995;17:523–46.
[39] Hatami K, Bathurst RJ. Effect of structural design on fundamental frequency of reinforced-soil retaining walls. Soil Dyn Earthq Eng 2000;19(3):137–57.
[40] Helwany SMB, Budhu M, McCallen D. Seismic analysis of segmental retaining walls. I: model verification. J Geotech Geoenviron Eng ASCE 2001;127(9):741–9.
[41] Ling HI, Liu H, Kaliakin VN, Leshchinsky D. Analyzing dynamic behavior of geosynthetic-reinforced soil retaining walls. J Eng Mech ASCE 2004;130(8):911–20.
[42] Ling HI, Liu H, Mohri Y. Parametric studies on the behavior of reinforced soil retaining walls under earthquake loading. J Eng Mech ASCE 2005;131(10):1056–65.
[43] Liu H. Analyzing the reinforcement loads of geosynthetic-reinforced soil walls subject to seismic loading during the service life. J Perform Constr Facil ASCE 2009;23(5):292–302.
[44] Ling HI, Yang S, Leshchinsky D, Liu H, Burke C. Finite-element simulations of full scale modular-block reinforced soil retaining walls under earthquake loading. J Eng Mech ASCE 2010;136(5):653–61.
[45] Liu H, Wang X, Song E. Reinforcement load and deformation mode of geosynthetic reinforced soil walls subject to seismic loading during service life. Geotext Geomembranes 2011;29(1):1–16.
[46] Liu H, Ling HI. Seismic responses of reinforced soil retaining walls and the strain softening of backfill soils. Int J Geomech 2012;12(4):351–6.
[47] Liu H, Yang G, Ling HI. Seismic response of multi-tiered reinforced soil retaining walls. Soil Dyn Earthq Eng 2014;61–62:1–12.
[48] Ren FF, Zhang F, Xu C, Wang G. Seismic evaluation of reinforced-soil segmental retaining walls. Geotext Geomembranes 2016;44(4):604–14.
[49] Corfdir A, Bourgeois E, Payeur JB. Numerical simulation of the response of a reinforced wall to a high speed train passage. Int J Numer Anal Methods Geomech 2017;41(11):1285–303.
[50] Murali KA, Bhattacharjee A. Behavior of rigid-faced reinforced soil-retaining walls subjected to different earthquake ground motions. Int J Geomech 2017;17(1):1–14.
[51] Pain A, Choudhury D, Bhattacharyya SK. Effect of dynamic soil properties and frequency content of harmonic excitation on the internal stability of reinforced soil retaining structure. Geotext Geomembranes 2017;45(5):471–86.
[52] Ramezani MS, Ghanbari A, Hosseini SAA. Analytical method for calculating natural frequencies of geosynthetic-reinforced wall with full-height concrete facing. Geosynth Int 2017;24(1):1–13.
[53] Liu H, Hung C, Cao J. Relationship between Arias intensity and the responses of reinforced soil retaining walls subjected to near-field ground motions. Soil Dyn Earthq Eng 2018;111:160–8.
[54] Qin C, Chian SC. Seismic stability of geosynthetic-reinforced walls with variable excitation and soil properties: a discretization-based kinematic analysis. Comput Geotech 2018;102:196–205.
[55] Ren F, Zhang F, Wang G, Zhao Q, Xu C. Dynamic assessment of saturated reinforced-soil retaining wall. Comput Geotech 2018;95:211–30.
[56] Ling HI, Leshchinsky D. Effects of vertical acceleration on seismic design of geosynthetic-reinforced soil structures. Geotechnique 1998;48(3):347–73.
[57] Nimbalkar SS, Choudhury D, Mandal JN. Seismic stability of reinforced-soil wall by pseudo-dynamic method. Geosynth Int 2006;13(3):111–9.
[58] Choudhury D, Nimbalkar SS, Mandal JN. External stability of reinforced soil walls under seismic conditions. Geosynth Int 2007;14(4):211–8.
[59] El-Emam MM. Experimental verification of current seismic analysis methods of reinforced soil walls. Soil Dyn Earthq Eng 2018;113:241–55.
[60] Zhang F, Gao Y, Leshchinsky D, Yang S, Dai G. 3D effects of turning corner on stability of Geosynthetic-Reinforced Soil Structures. Geotext Geomembranes 2018;46(4):367–76.
[61] Berg RR, Christopher BR, Samtani NC. Design of mechanically stabilized earth walls and reinforced slopes. Rep. No. Federal highway administration (FHWA)-NHI-10-024 Vol. vol. I and NHI-10-025 Vol II, Washington, DC.
[62] DGGT (Die Deutsche Gesellschaft für Gentherapie). Recommendations for design and analysis of earth structures using geosynthetic reinforcements - EBGEO. Berlin, Germany: Wilhelm Ernst & Sohn; 2011.
[63] Hatami K, Bathurst RJ. Effect of structural design on fundamental frequency of reinforced-soil retaining walls. Soil Dyn Earthq Eng 2000;19(3):137–57.
[64] Nouri H, Fakher A, Jones CJFP. Evaluating the effects of the magnitude and amplification of pseudo-static acceleration on reinforced soil slopes and walls using the limit equilibrium Horizontal Slices Method. Geotext Geomembranes 2008;26(3):263–78.
[65] Bathurst RJ, Hatami K. Seismic response analysis of a geosynthetic reinforced soil retaining wall. Geosynth Int 1998;5(1–2):127–66.
[66] Jibson RW. Predicting earthquake-induced landslide displacements using Newmark's sliding block analysis. Transp Res Rec 1993;1411:9–17.
[67] Loh CH, Lee ZK, Wu TC, Peng SY. Ground motion characteristics of the Chi-Chi earthquake of 21 September 1999. Earthq Eng Struct Dyn 2000;vol. 29(6):867–97.
[68] Ling HI, Leshchinsky D. Failure analysis of modular-block reinforced-soil walls during earthquakes. J Perform Constr Facil ASCE 2005;19(2):117–23.
[69] Shekarian S, Ghanbari A, Farhadi A. New seismic parameters in the ana-lysis of retaining walls with reinforced backfill. Geotext Geomembranes 2008;26(4):350–6.
[70] Basha BM, Babu GLS. Seismic reliability assessment of internal stability of reinforced soil walls using the pseudo-dynamic method. Geosynth Int 2011;18(5):221–41.

[71] Vahedifard F, Leshchinsky D, Meehan CL. Relationship between the seismic coefficient and the unfactored geosynthetic force in reinforced earth structures. J Geotech Geoenviron Eng ASCE 2012;138(10):1209–21.
[72] Huang CC, Wang WC. Seismic displacement of a geosynthetic-reinforced wall in the 1995 Hyogo-ken nambu earthquake. Soils Found 2005;45(5):1–10.
[73] Zhao L, Cheng X, Dan H, Tang Z, Zhang Y. Effect of the vertical earthquake component on permanent seismic displacement of soil slopes based on the nonlinear Mohr–Coulomb failure criterion. Soils Found 2017;57(2):237–51.
[74] Zarnani S, El-Emam MM, Bathurst RJ. Comparison of numerical and analytical solutions for reinforced soil wall shaking table tests. Geomech and Eng 2011;3(4): 291–321.
[75] Lee KZZ, Chang NY, Ko HY. Numerical simulation of geosynthetic-reinforced soil walls under seismic shaking. Geotext Geomembranes 2010;28(4):317–34.
[76] Bathurst RJ, Miyata Y, Nernheim A, Allen AM. Refinement of K-stiffness Method for geosynthetic-reinforced soil walls. Geosynth Int 2008;15(4):269–95.
[77] Allen TM, Bathurst RJ. Improved simplified method for prediction of loads in reinforced soil walls. J Geotech Geoenviron Eng 2015;141(11):04015049.
[78] Chan AHC. User manual for Diana-Swandyne-II. Glasgow: Dept. of Civil Engineering, Univ. of Glasgow; 1993.
[79] Liu H. Finite Element simulation of the response of geosynthetic-reinforced soil walls. New York: Columbia University; 2002.
[80] Ling HI, Liu H. Pressure dependency and densification behavior of sand through a generalized plasticity model. J Eng Mech ASCE 2003;129(8):851–60.
[81] Bathurst RJ, Cai Z. In-isolation cyclic load-extension behavior of two geogrids. Geosynth Int 1994;1(1):1–19.
[82] Desai CS, Zaman MM, Lightner JG, Siriwardane HJ. Thin-layer element for interface and joints. Int J Numer Anal Methods Geomech 1984;8:19–43.
[83] Burke C. Full-scale shaking table tests and Finite Element analysis of reinforced soil retaining walls. New York: Columbia University; 2004.
[84] Ling HI. A critical review of full-scale shaking table tests conducted on reinforced soil retaining walls. Arhqa Ran Dgn. 2003. p. 491–510.
[85] Hatami K, Bathurst RJ. Numerical model for reinforced soil segmental walls under surcharge loading. J Geotech Geoenviron Eng ASCE 2006;132(6):673–84.
[86] Hossain S, Omelchenko V, Mahmood T. Case history of geosynthetic reinforced segmental retaining wall failure. Electron J Geotech Eng 2009:14. Bundle C: 15.